International Journal of Fatigue 186 (2024) 108361

Contents lists available at ScienceDirect

International Journal of Fatigue

journal homepage: www.elsevier.com/locate/ijfatigue

Very high cycle fatigue assessment of thermoplastic-based hybrid fiber metal laminate by using a high-frequency resonant testing system

Selim Mrzljak [a,*], Maik Trautmann [b], Guntram Wagner [b], Frank Walther [a]

[a] Chair of Materials Test Engineering (WPT), TU Dortmund University, Dortmund, Germany
[b] Institute of Material Science and Engineering (IWW), Chemnitz University of Technology, Chemnitz, Germany

ARTICLE INFO

Keywords:
High-frequency resonant testing
Very high cycle fatigue
Fiber metal laminate
Thermoplastic
Post-stretching
Digital image correlation

ABSTRACT

The prolonged fatigue lifetime of fiber metal laminates (FML) compared to monolithic metals is a key aspect for safety-relevant components, where detailed knowledge about the fatigue properties up to the very high cycle fatigue (VHCF) regime is necessary. For thermoplastic-based FMLs, offering formability, recyclability, and mass production due to short consolidation cycle times, this knowledge needs to be established.

In this study, FML containing AA6082 sheets and unidirectional glass and carbon fiber-reinforced polyamide 6 was investigated. Fatigue tests up to max. 10^9 cycles were conducted on a servo-hydraulic and a high-frequency resonant fatigue testing system with frequencies of 10 Hz and 1,000 Hz. Frequency-induced self-heating was evaluated and limited using air-cooling to maintain the matrix properties. Fatigue progress was monitored through high-speed optical deformation analysis.

Compared to HCF loads, VHCF loads lead to reduced crack and delamination occurrence. Changes in microstructure are dominated by singular crack initiation and propagation within the aluminum. The FML's S-N curve shows a significant flattening from the HCF to the VHCF regime, simplifying the predictability of the fatigue life. By using post-stretching, the VHCF strength can be increased by over 60 %, making this thermoplastic-based FML a considerable competitor in the field of FML.

1. Introduction

Compared to monolithic metal sheets, fiber metal laminates (FML) offer the benefits of prolonged and sequential fatigue damage evolution [1–5]. E.g., tension–tension load in laminate plane direction leads initially to crack formation in the metal sheets, followed by interlaminar damage development within the metal-polymer interfaces until failure of the metal, after which the load still can be transferred over the remaining fiber-reinforced polymer (FRP) layers [6,7]. The superior performance and monitorability of FML proved its applicability already for i.e., the aeromotive industry [3,8]. Established and thoroughly researched representatives of FMLs contain e.g., aluminum sheets and thermoset matrix systems, such as ARALL (aramid fiber-reinforced epoxy [9]), GLARE (glass fiber-reinforced epoxy [10]), and CARALL (carbon fiber-reinforced epoxy [11]). But also, FMLs with thermoplastic-based FRP are present, offering the possibilities of improved formability [12–14], recyclability, and mass production due to short consolidation cycle times [12,15–17]. However, the knowledge about the mechanical properties of thermoplastic-based FMLs, especially considering fatigue [18–22], is limited compared to thermoset-based FMLs.

In general, a detailed holistic characterization of the mechanical properties including very high cycle fatigue (VHCF) is essential to evaluate their suitability for practical applications, which is associated with great time and financial effort. To achieve feasible FML qualification for long-term applications with regard to reliable and thus sustainable component design for VHCF lifetime, methods for short-term characterization are necessary. Extrapolation of characteristic mechanical properties for the FML and the individual laminate materials, determined in the high cycle fatigue (HCF) regime based on, e.g., conventional servo-hydraulic testing systems (testing frequency (f) of 0.5 to around 100 Hz) [15,23,24], or resonance testing systems (f of 50 to around 200 Hz) [15,25], is only suitable to a limited extent. Deviations regarding the lifetime between HCF and VHCF regimes can occur, including changes in the S-N curve slope, both for aluminum [26,27] and FRP [24,28]. Very high testing frequencies, as with ultrasonic testing at f = 20 kHz, enable short testing durations but result in difficult controllable self-heating, that can generally only be tamed by the use of extensive cooling and pulse/pause cycles [27–33]. Latter lead to

* Corresponding author.
E-mail address: selim.mrzljak@tu-dortmund.de (S. Mrzljak).

https://doi.org/10.1016/j.ijfatigue.2024.108361
Received 12 February 2024; Received in revised form 6 April 2024; Accepted 27 April 2024
Available online 28 April 2024

inconsistent loading due to the start and stop phases of the oscillation cycles, which is amplified by the restriction of displacement-controlled testing and thus stiffness-dependent loading. Moreover, the geometries for the tested specimens are limited, since the specimen needs a shape suitable for the ultrasonic system for testing in resonance. Servo-hydraulic [34–38] and resonance testing systems [24,39,40] with f ≈ 1,000 Hz are alternatives since the testing durations for equal numbers of cycles can be similar to ultrasonic systems, considering the usage of pulse-pause. These systems offer the advantages of stress-controlled testing and less restrictive specimen geometries with reduced self-heating. While they have been used for metals and FRP, insufficient results are available for FMLs.

One aspect to be taken into account during such short-term testing is the reduced test duration due to increased testing frequencies, which results not only in increased temperature input but also in increased strain rate. This all together can influence the mechanical properties of the laminate and its components. In the case of aluminum alloys applied under fatigue loading conditions with occurring crack-opening (e.g., reversed or tension–tension loading), it was shown that higher testing frequencies (f = 20 kHz) can result in improved fatigue life [25–27,40–43]. However, this is not attributed to increased strain rate, but to shortened hydrogen exposure of the crack tips during crack formation and evolution, which slows down crack propagation with respect to the number of cycles. For polymer components, an increased strain rate leads to a reduction in loading time and therefore reduced creep deformation during fatigue load, which is counteracted by the increased self-heating. As long as the strain rate-dependent self-heating is accounted for, polymers in general exhibit a prolonged fatigue life with increased strain rate [44–47], but this has little impact on fiber composites [23,24,48], as increased strain rate does not significantly increase the fatigue life of the primarily loaded fibers. On the contrary, if self-heating is not limited, the increased temperatures reduce the interface properties and lead to earlier damage in matrix-dominated areas [49–51], especially at higher loads [33,52–54].

In addition, due to different coefficients of thermal expansion, thermally induced residual stresses are a major factor for the FMLs' fatigue properties. Such can occur within thermoplastic-based FMLs to a higher magnitude compared to a thermoset variant since it is consolidated under higher temperatures. While the FRP experiences compressive residual stresses, the aluminum sheets experience tensile residual stresses which reduce fatigue life. This can be intensified by cooler ambient conditions, increasing the residual stresses further [55]. Post-stretching, describing the process of stretching the FML after consolidation to reduce or revert the residual stress state [56–59], can effectively increase fatigue performance [30,57,60], but its applicability for thermoplastic-based FML has not been investigated yet [20].

In this study, the application of high-frequency resonant testing with f ≈ 1,000 Hz for the characterization of FML fatigue properties is evaluated using a laminate consisting of aluminum sheets and polyamide 6 (PA6)-based GFRP as well as CFRP. Besides general applicability, one key aspect is the degree of comparability of the fatigue results generated at f ≈ 1,000 Hz and lower frequencies, since influences such as reduced testing time, strain rate and self-heating can affect the FML's performance. In addition to thermography for temperature recording, digital image correlation is used for monitoring fatigue-induced deformation and damage processes with a frame rate of 25 kHz using high-speed cameras. The focus is on monitoring the crack development present in the aluminum sheets. Using the testing setup, the fatigue properties of the FML in the initial state after the consolidation as well as after post-stretching are investigated using different testing strategies.

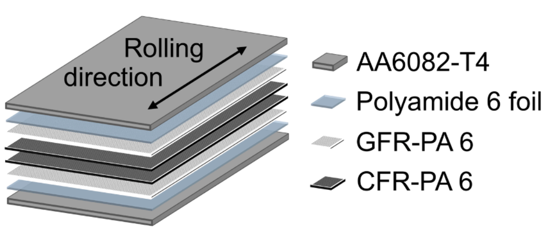

Fig. 1. Schematic visualization of thermoplastic-based fiber metal laminate setup with a 2/1 metal-to-FRP configuration.

2. Material and methods

2.1. Fiber metal laminate material and manufacturing

For the FML a hybrid combination of three materials is used. It consists of AA6082 T4 sheets with an initial thickness of 0.5 mm as the metal part and glass as well as carbon fiber-reinforced polyamide 6 with unidirectional fiber alignment. Carbon fibers are chosen for higher residual strength of the FML after aluminum failure, and glass fibers are implemented to achieve a finer-graded transition in terms of thermal expansion between the carbon fibers and the aluminum, while also increasing corrosion resistance [7]. Fig. 1 shows the investigated 2/1 metal-to-FRP laminate structure with a total of four FRP layers. The rolling direction of the metal sheets as well as the orientation of the unidirectional fibers are indicated.

Before the consolidation of the FML, the metal sheets were mechanically blasted to enhance the interface capabilities, increasing the arithmetic mean roughness to 5.74 μm [17] while reducing the sheet thickness to 0.49 mm. As FRP pre-consolidated CePreg-foils (Cetex Institut gGmbH, Chemnitz, Germany), processed with a fiber-foil-tape-unit continuously into a width of 300 mm [12] with a resulting fiber volume fraction of 0.5, are used. These consist of two 40 μm thick polyamide 6 foils (mf-Folien GmbH, Kempten, Germany) and TURov 4588 (Nippon Electric Glass Co. Ltd., Tokyo, Japan) for the glass fibers and ZOLTEK PX35 50 K (ZOLTEK Corporation, Bridgeton, NJ, USA) for the carbon fibers. To minimize pore formation during the consolidation, all CePreg-foils are dried in an oven at 80 °C for one hour and an additional PA6 foil is placed between the aluminum and the FRP. Consolidation of the FML is performed using a Collin PM300 (COLLIN Lab & Pilot Solutions GmbH, Maitenbeth, Germany) thermal press with a dipping-edge tool (Fig. 2a), following the process cycle shown in

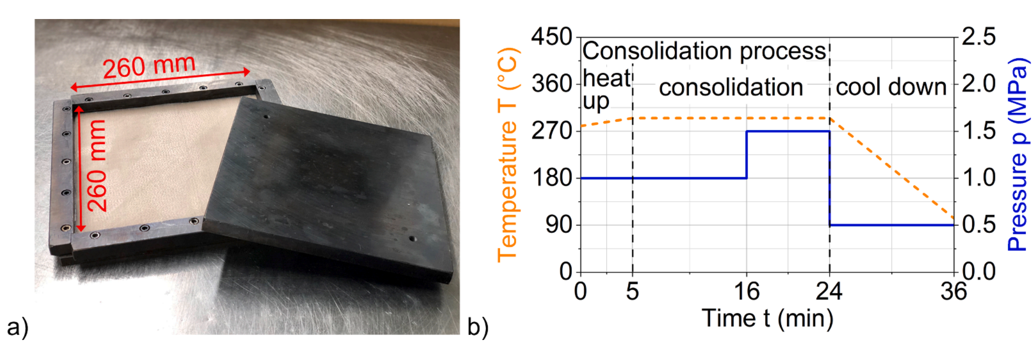

Fig. 2. A) dipping edge tool and b) process cycle for thermoplastic-based fiber metal laminate consolidation [22,61].

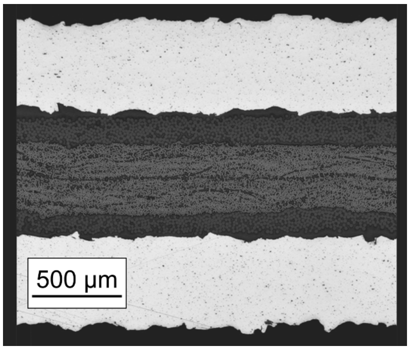

Fig. 3. Light microscopy cross-sectional image of thermoplastic-based fiber metal laminate.

Fig. 2b).

The microstructure of the consolidated FML is shown in Fig. 3 as a cross-sectional image (perpendicular to the fibers). No significant pore formation, nor delamination within the metal-polymer interface is visible, while also achieving a good mechanical interlocking by undercut areas. Further, a consistent and homogeneous distribution of the single FRP layers is apparent. The GFRP layers isolate the CFRP layers successfully from the aluminum, eliminating the possibility of galvanic corrosion (except at the cutting edges, if not isolated from a surrounding electrically conductive medium).

2.2. Specimen

After the consolidation rectangular-shaped specimens with a width of 15 mm were cut out via micro water-jet cutting based on type A from ISO 527–5. The total specimen length was 160 mm with 40 mm long protection tabs (leaving a measuring length of L_2 = 80 mm) for investigations within the HCF regime, while it was reduced to 96 mm with 2 × 33 mm protection tabs (leaving a measuring length of L_2 = 30 mm) for the VHCF regime due to displacement limitations of the high-frequency resonant testing system. The remaining measuring lengths of the specimens were speckled with a stochastic pattern to enable digital image correlation (DIC) measurements.

The ultimate tensile strength (UTS) of the FML is measured at 625 MPa [17].

2.3. Fatigue testing setup and strategy

For investigations within HCF and VHCF regimes, two different testing setups were applied to achieve suitable testing frequencies regarding self-heating and economically viable testing durations.

2.3.1. High cycle fatigue regime

The testing configuration for the HCF regime (up to 2 × 10^6 cycles) proved in previous investigations [17,22,61] its suitability and is shown in Fig. 4. Constant amplitude tests (CAT) were conducted on a servo-hydraulic testing system EHF-EV50 (Shimadzu Corporation, Kyoto, Japan, maximum force F_{max} ± 50 kN) with a sinusoidal load-time function and a stress ratio of R = 0.1. For the limitation of self-heating according to ISO 13003, a testing frequency of f = 10 Hz was applied. For deformation and crack detection, a Limess Q400 DIC system (Limess Messtechnik und Software GmbH, Krefeld, Germany) was used alongside a conventional Shimadzu TCK 1 LH tactile extensometer (L_0 = 25 mm, ΔL = 1 mm). It contains 5 Megapixel cameras, equipped for front aluminum sheet surface measurements with i) a Schneider Kreuznach lens XENOPLAN 2.0/28–0901, 28 mm focal length, and for FML edge measurements with ii) a Ricoh TV lens FL-CC7528-2 M, 75 mm focal length with 95 mm of extension tubes. Captioning deformation states was triggered at maximum stress for selected cycles to reduce data. Temperature measurements on the aluminum surface were conducted with a thermoIMAGER TIM 400 thermographic camera (Micro-Epsilon Messtechnik GmbH & Co. KG, Ortenburg, Germany). Further, the dynamic stiffness (C_{dyn}) was recorded, which represents the change of force divided through the change of piston displacement: $(F_{max} - F_{min})/(s_{max} - s_{min})$.

2.3.2. Very high cycle fatigue regime

For the VHCF regime (up to 1 × 10^9 cycles) a high-frequency resonant testing system Rumul GIGAFORTE 50 (Russenberger Prüfmaschinen AG, Neuhausen am Rheinfall, Switzerland, maximum force amplitude F_a ± 25 kN, maximum force F_{max} ± 50 kN) with f ≈ 1,000 Hz was utilized (Fig. 5). To limit the self-heating in accordance with ISO 13003, compressed air (room temperature) was applied for cooling with the help of flat fan air nozzles at a pressure of 0.2 MPa. The testing system is limited to displacement amplitudes of $s_{a,max}$ ± 0.1 mm. CAT, as well as multiple amplitude tests (MAT) [17,21], were conducted at a stress ratio of R = 0.1. Due to the higher testing frequency, a high-speed camera system GOM ARAMIS HHS 6400 (Carl Zeiss GOM Metrology GmbH, Braunschweig, Germany) was utilized for DIC analysis of deformation and crack detection, as well as strain measurement. The system includes Photron Nova Fastcam 1 Megapixel cameras (framerate up to 6,400 Hz at full resolution), which were configured for a frame rate of 25 kHz at a resolution of 0.3 Megapixel. High-power GOM light projectors (Rev. 01) were used to reach the necessary shutter speeds. These were equipped with Titanar B lenses, 75 mm focal length, with 10 mm extension tubes for front aluminum sheet surface measurements. Captioning deformation states was triggered using a self-written LabView module, which enabled the recording of selected cycles (to reduce data) with 25 images each. Temperature measurements on the specimen surface were conducted using an Infratec ImageIR 8800 thermographic

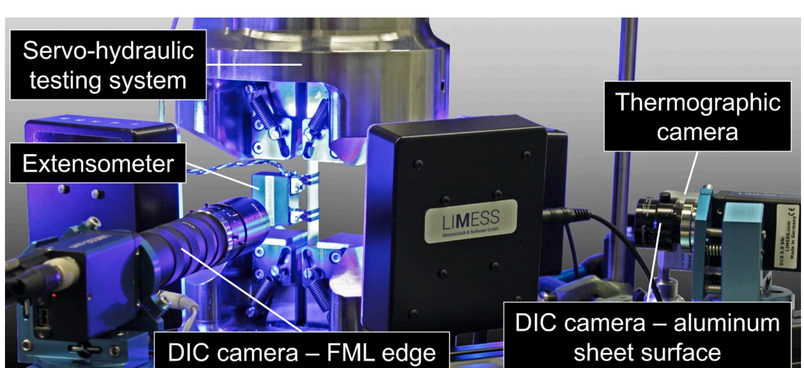

Fig. 4. Illuminated fatigue testing setup on a servo-hydraulic testing system with cameras perpendicular to the specimen (recording the aluminum sheet surface and fiber metal laminate (FML) edge), a thermographic camera, and a tactile extensometer [17].

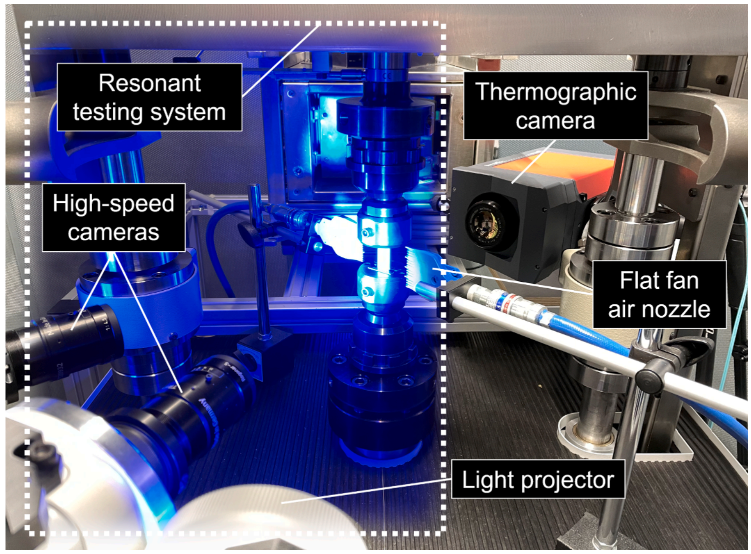

Fig. 5. Fatigue testing setup on a high-frequency resonant testing system with high-speed cameras (recording the aluminum sheet surface), and a thermographic camera. The dotted area shows the setup with illumination.

camera (InfraTec GmbH Infrarotsensorik und Messtechnik, Dresden, Germany).

3. Results and discussion

3.1. Influence of specimen length adjustment for VHCF analysis

The fatigue life of the thermoplastic-based FML was determined for the HCF regime on the servo-hydraulic testing system using the specimens with $L_2 = 80$ mm specified in Section 2.2. Due to the limited displacement amplitude of the high-frequency resonant testing system, a maximum stress of 80 MPa could not be exceeded for the investigated FML with a measuring length L_2 of 80 mm. This leads to the necessity of a reduced L_2 for a timely efficient characterization of the FML within the VHCF regime. Therefore, considering the occurring strains in the HCF regime, the measuring length was reduced by approx. 60 % from 80 to 30 mm, enabling testing of the complete FML fatigue life (from aluminum to total failure) within the VHCF regime. As Fig. 6 shows as an example for a maximum stress of 265 MPa (HCF regime), a reduction of the measuring length does not lead to significant differences in the course of the stiffness development. The time of aluminum cracking, starting with a reduction of stiffness and reaching through the whole specimen width by the time the stiffness surpasses its inflection point, as well as the time of total failure of the FML, take place in comparable time periods.

As a consequence, the occurring damage should be comparable. This is confirmed by the DIC deformation images of the related experiments (Fig. 7), which represent the deformation state close to failure. Besides an overall identical strain development, similar amounts of aluminum cracks, as well as interlaminar delamination propagation between the aluminum and FRP layers and intralaminar strain accumulation within the FRP layers, are apparent. Therefore, the use of a specimen with a reduced measuring length of 30 mm is considered valid.

3.2. High cycle fatigue damage evolution and mechanisms

The stiffness degradation as well as DIC deformation analysis can further be used to establish knowledge about the HCF-related damage evolution and mechanisms. Fig. 8 shows the normalized stiffness development during maximum stresses of 265, 200, 150, and 100 MPa. In general, a consistent maximum stress-dependent behavior is visible. For higher maximum stresses, at the start of the test plastic deformation-

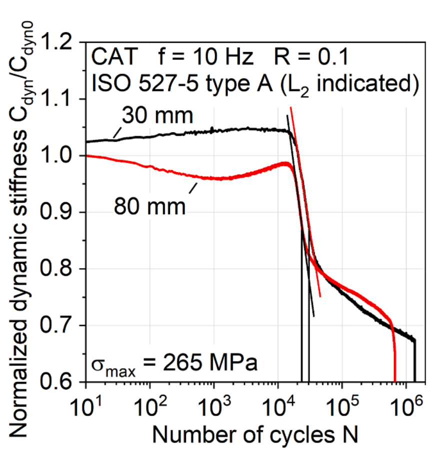

Fig. 6. Constant amplitude test at maximum stress of 265 MPa on specimens with measuring lengths L_2 of 80 and 30 mm. The time of complete aluminum crack is indicated for both lengths.

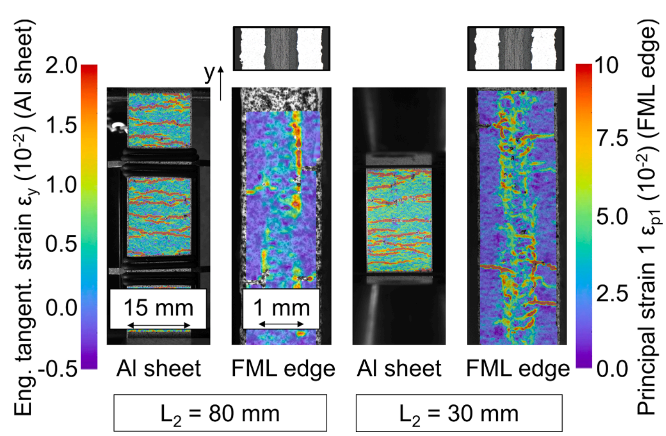

Fig. 7. Digital image correlation-based deformation states from the aluminum sheet and fiber metal laminate (FML) edge, gained from constant amplitude test experiments at maximum stress of 265 MPa on specimens with measuring lengths L_2 of 80 and 30 mm. The images represent the deformation and damage states at maximum stress for cycle 6×10^5 (close to failure).

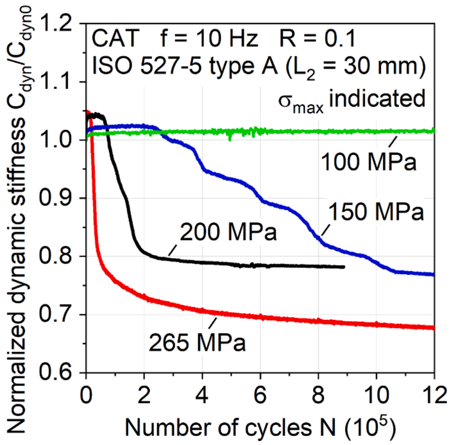

Fig. 8. Dynamic stiffness development during constant amplitude tests at maximum stresses of 265, 200, 150, and 100 MPa on specimens with a measuring length L_2 of 30 mm.

induced cyclic hardening of the aluminum sheet can be observed, visible by the increase in stiffness. The intensity and duration of the cyclic hardening depends on the maximum stress, taking place reduced and in a longer time frame for lower maximum stress. Aluminum crack-related decrease in stiffness, after the process of cyclic hardening, is postponed and prolonged with lower maximum stress, not being recognizable anymore at 100 MPa within the investigated 2×10^6 cycles.

Fig. 9 shows exemplary damage states, where the course of stiffness flattens after the reduction to a nearly saturated state. Correlating to the reduced stiffness decrease with reduced maximum stress the number and density of cracks within the aluminum sheet is reduced for comparable fatigue lifetime. The same applies to interlaminar delamination growth and intralaminar strain accumulation. At the beginning of the stiffness decrease, cracks develop in a reduced manner compared to the final state when the stiffness reduction is saturating. Extrapolating this behavior to fatigue life during VHCF loads, the event of singular crack development is to be assumed, which still will lead to comparable stiffness development, just in a prolonged time frame. Therefore, the application of the same characterization technique for the VHCF regime seems justified, enabling a conclusive analysis of the mechanical properties for all numbers of cycles.

3.3. Self-heating at 1,000 Hz testing frequency

Applying f ≈ 1,000 Hz for investigations within the VHCF regime results in increased strain rate, and self-heating, which are serious threats regarding the comparability of the results gained within the HCF regime with f = 10 Hz. As stated in Section 1, strain rate has a lifetime-extending effect on aluminum as well as fiber-reinforced polymers and can only be investigated by the application of different testing frequencies for equal numbers of cycles. Effects of self-heating on the other hand can be investigated by equalizing the temperature conditions of the specimens, by adjusting the specimen temperature through the environment. In the case of the FML, the aluminum sheets with their multiple times higher thermal conductivity compared to the inner FRP [62] act as heat sinks, reducing the self-heating-induced increase in temperature. Further, the surface-to-volume ratio of around 1.25 is beneficial for heat exchange. Fig. 10 shows the surface temperature measured either for the FML (Fig. 10 a) as well as for the FRP (Fig. 10 b, representing the case when the aluminum fails and does not contribute to load bearing) for maximum stresses up to 150 MPa. As is visible in Fig. 10 a,b), air cooling helps significantly with cooling down the laminate structure and increasing the testable stress range, and is necessary for the characterization of the total FML fatigue life considering the FRP-related temperature. Considering the intact FML, measurements up to 180 MPa would be possible without the change in temperature exceeding 10 K. The aluminum sheets are the limiting factor. To verify, that temperature measurements taken on the surface of the material are not impeded by the overlying flow of cooling air, measurements were taken on one side of the specimen, being isolated from cooling air, yielding results lying in-between measurements with and without cooling air.

Considering the changes in temperature related to the displacement amplitude (Fig. 10 c,d) it becomes evident, that for investigations on the intact FML, the difference between the surface to inner temperature of the FRP is negligible. Even when considering the total failure of the aluminum sheets, still there are no significant changes in temperature with the applied cooling solution. For the latter, only excess of the maximum displacement amplitude is the limiting factor considering testable maximum stresses in the VHCF regime at f ≈ 1,000 Hz. Interestingly, surpassing a maximum stress of around 100 MPa, marked by the vertical red line in Fig. 10 c), leads to a disproportionate increase in temperature due to the plastic deformation of the aluminum, indicating a possible fatigue strength for the VHCF regime.

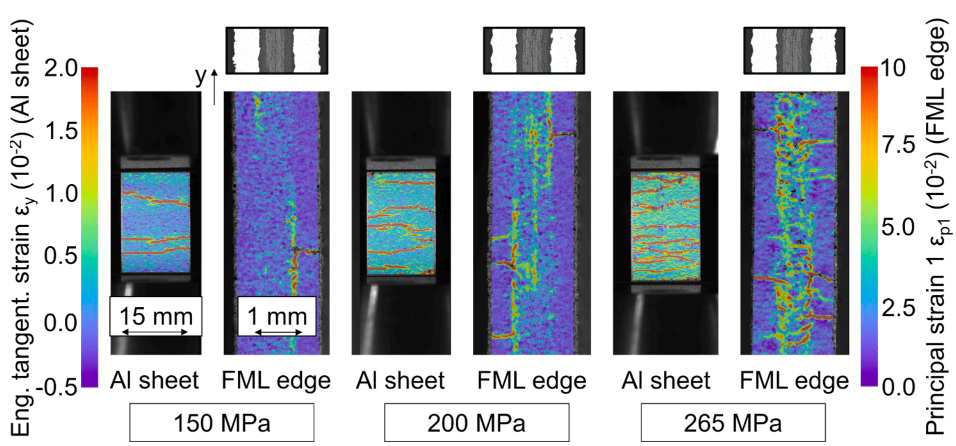

Fig. 9. Digital image correlation-based deformation states from the aluminum sheet and fiber metal laminate (FML) edge, gained from constant amplitude test experiments at maximum stresses of 265, 200, and 150 MPa on specimens with a measuring length L_2 of 30 mm. The images represent the deformation and damage states at maximum stress for cycles 7×10^5 (200 MPa) and 1.25×10^6 (265 and 150 MPa).

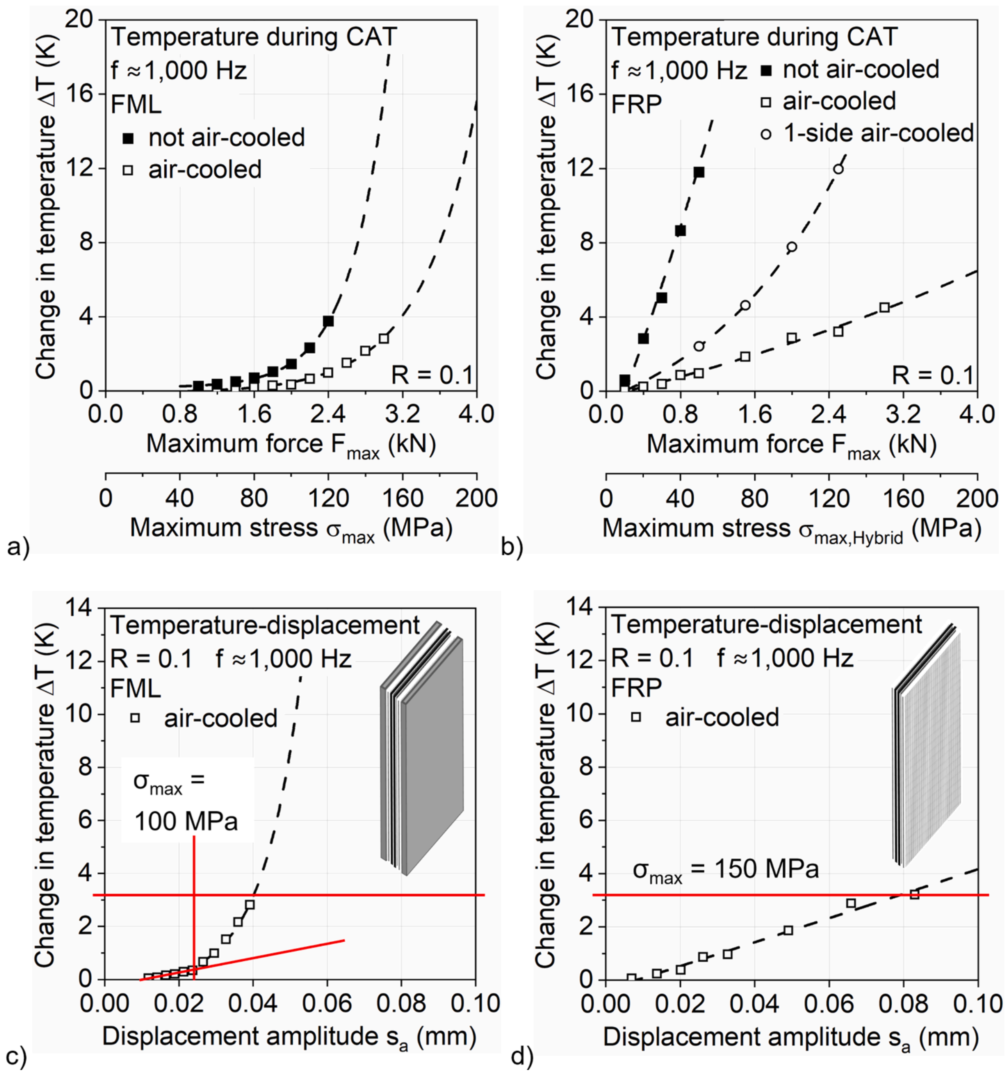

Fig. 10. Relationship between (a,b) load- and (c,d) displacement-dependent change in temperature of the (a,c) fiber metal laminate (FML) and (b,d) fiber reinforced polymer (FRP) (latter represents the case of the FML with failed aluminum sheets) for ≈ 1,000 Hz of testing frequency.

3.4. Multiple amplitude testing for very high cycle fatigue strength estimation

To estimate the fatigue strength of the thermoplastic-based FML, MATs were conducted, enabling a short-term impression about the aluminum crack initiation and evolution under numbers of cycles higher than 2×10^6. Fig. 11 shows such a test starting at maximum stress of 80 MPa (based on the temperature increase/plastic deformation observations in Fig. 10 c with a step width of 10^7 cycles, after which the maximum stress is increased by 10 MPa. The testing frequency at the start (f_{start}) of the MAT was 990 Hz. Associated DIC deformation images are illustrated, visualizing the aluminum crack initiation, evolution, and crack-related delamination growth. Confirming the presumptions by earlier results, aluminum failure is initiated at 100 MPa after around 2.5 $\times 10^6$ cycles. As before, the FML damage state is measurable using the dynamic stiffness, but also the change in testing frequency (Δf) and the total strain (ε_t), which is corroborated by the DIC deformation images to the same degree as it was for the HCF regime. The damage evolution in the VHCF regime shows reduced crack initiation and delamination with slower propagation. Moreover, increasing maximum stress during the MAT introduces not only delamination growth but also new cracks. This supports the validity of the relationship between maximum stress and occurring damage mechanisms and damage amount observed in the HCF regime (compare Section 3.2) up to the VHCF regime.

3.5. Very high cycle fatigue properties

With the established groundwork CATs were conducted upwards of a maximum stress of 80 MPa, to generate information about the fatigue life of the FML regarding the aluminum sheets as well as the total FML. Since the initial HCF regime tests were conducted in a range of maximum stresses, where a total failure of the FML was reached within 2×10^6 cycles, only limited results were gathered about the aluminum crack occurrence within the HCF regime. To enable the evaluation of the transition between the HCF and VHCF regime as well as the comparison of the influence of f = 10 Hz and ≈ 1,000 Hz, supplementary experiments at maximum stresses below 225 MPa were conducted on the servo-hydraulic testing system to complement the results of aluminum cracking up to around 3×10^6 cycles. The fatigue strength of the FML is visualized in Fig. 12, divided into the cracking of the aluminum layers (triangles) and the total failure of the FML (circles). Filled data points represent experiment results gathered on the servo-hydraulic testing

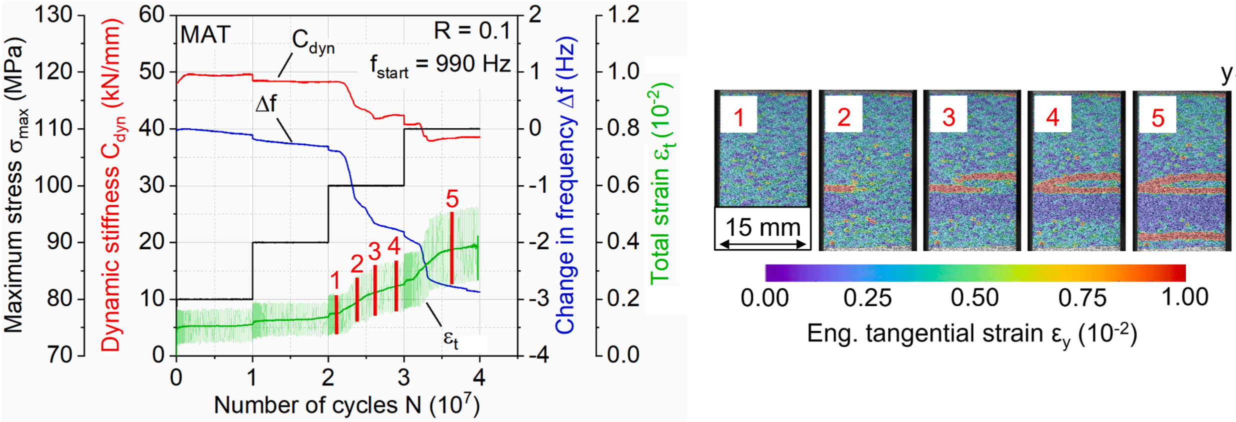

Fig. 11. Multiple amplitude test using a testing frequency of ≈ 1,000 Hz, starting at a maximum stress of 80 with a step width of 10^7 cycles, after which the maximum stress is increased by 10 MPa until 110 MPa. Events of crack initiation and evolution within the front aluminum sheet are marked with numbers and illustrated using digital image correlation deformation images, which represent the state at maximum stress.

system, while the contour-bordered data points were obtained on the high-frequency resonant testing system. The fatigue life results gathered at f ≈ 1,000 Hz are consistent with the results from 10 Hz testing. This indicates that the effect of strain rate for this case is negligible. In general, the lower the maximum stress, the longer the fatigue life between aluminum cracking and failure of all laminate layers. Thus there is headroom regarding a fail-safe design of FML components since the fatigue life of the overall FML is many times that of the aluminum sheets. Further, a distinct change in the S-N curve slope is visible between the HCF and the VHCF regime, indicating that the fatigue strength of the FML, considering intact aluminum sheets, lies at around 90 MPa.

Fig. 13 shows an exemplary result of a CAT conducted at maximum stress of 150 MPa, illustrating the development of dynamic stiffness, change in testing frequency, and temperature. Three major changes in property development are visible, showing the initial decrease of stiffness due to aluminum cracking, followed by a plateau where cracks and interlaminar delamination progress, with a consecutive decrease due to failure of the GFRP layers after 80 % of the tested number of cycles (light microscopy image of the FML edge in Fig. 13). Even though the FML has lost its structural integrity, the remaining CFRP layers enable the laminate to still maintain the load (effective maximum stress of around 900 MPa) up to the run-out criteria of 10^9 cycles, proving their value regarding residual strength of the FML. The measured initial change in temperature is in accordance with the values gained from the preliminary investigations regarding the testing frequency. The second increase is attributed to the formation of interlaminar delamination, which leads to an increase in friction between the layers.

3.6. Lifetime enhancement through post-stretching

In Fig. 14 stress–strain curves are visualized for the aluminum sheet (red curves), the FML (blue curves), and the FML stretched until a nominal tensile stress of 300 MPa (leading to a total strain of 0.8 %) and unloaded (black curve), leaving a remaining total strain of 0.3 %. The thermally induced residual stresses in the FML are obvious when compared to the yield strength of the aluminum itself, seeing that the kink is lowered significantly from 120 to about 60 MPa. This is in accordance with the results of x-ray diffraction measurement results for the aluminum sheets in a similar TP-FML [20], where residual stresses between 50 and 60 MPa were found. By applying post-stretching, the plasticity of the aluminum is used to shift the area of the aluminum's compressive and tensile elastic behavior to a higher load, making it less prone to crack initiation within the span of this load. With regard to the

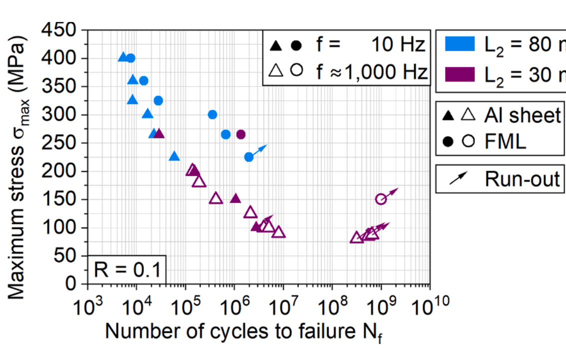

Fig. 12. S-N graph for thermoplastic-based fiber metal laminate (FML). Data points contain experimental results gained from servo-hydraulic 10 Hz (filled data points) and high-frequency resonant ≈ 1,000 Hz (contour-bordered data points) testing. Triangles represent aluminum sheet cracking and circle total failure of the FML.

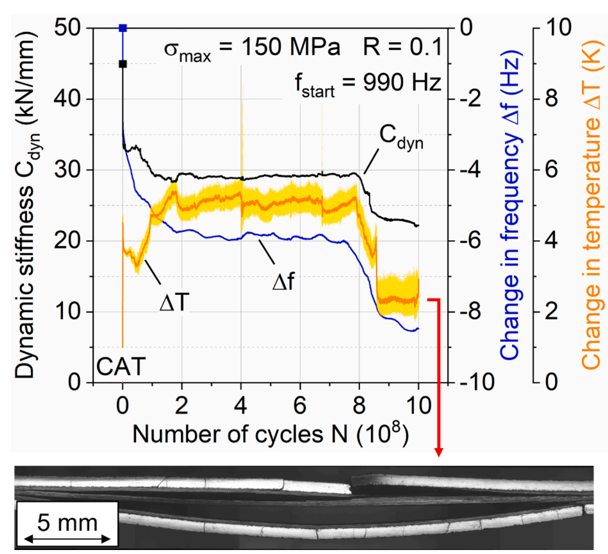

Fig. 13. Constant amplitude test at a maximum stress of 150 MPa and testing frequency of ≈ 1,000 Hz. Aluminum cracking takes place at the beginning of the test, while the failure of the GFRP layers follows after 80 % of the tested number of cycles, with only the CFRP layers remaining after 10^9 cycles (run-out), as is visible in the light microscopy image of the fiber metal laminate edge.

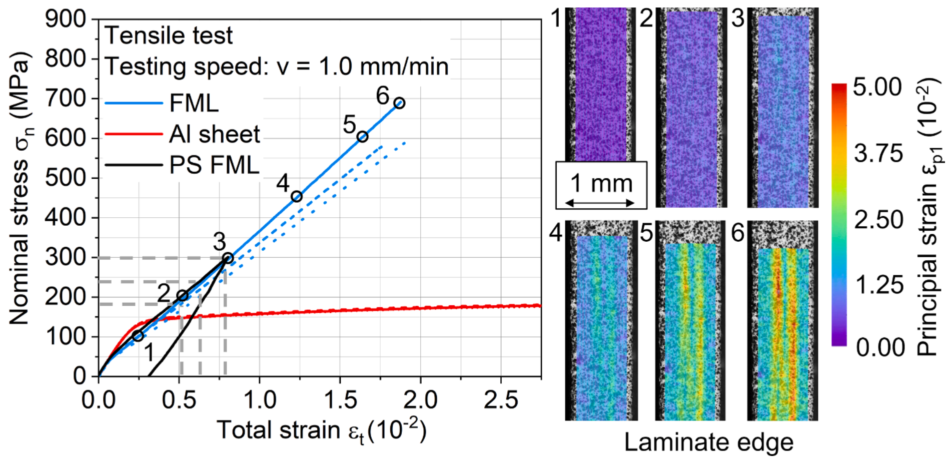

Fig. 14. Stress–strain curves for AA6082-T4 sheets (state after consolidation heat treatment) and the thermoplastic-based fiber metal laminate (FML). DIC deformation images of the FML edge are shown for strain states at selected nominal stresses. A curve of a post-stretched (PS) FML, up to 300 MPa, is overlayed.

interface capabilities of enduring plastic strain, for this FML around 300 MPa of tensile stress for post-stretching is seen as a permissible value since the interface strain between the layers is still almost homogenously distributed (Fig. 14 DIC image 3). For higher values, significant increases in interface strain occur, affecting the remaining interface adhesion due to interlaminar damage. As indicated, three different levels of post-stretching were applied for investigation regarding the performance of the FML within the VHCF regime: post-stretching up to 180, 240, and 300 MPa. The amount of post-stretching is deliberately specified in the form of the stress applied to the FML after consolidation, rather than strain. Using the latter, process-related deviations in the FRP content of the FML and therefore individual specimen stiffness (compare blue lines in Fig. 14, representing the variation between FML specimens) would lead to different stresses applied during post-stretching. This, in relation to the subsequently applied maximum stress during the fatigue test, would reduce comparability between specimens.

The effectiveness of post-stretching is demonstrated through the use of MATs (Fig. 15), comparing no post-stretching to 300 MPa of post-stretching. Post-stretching to 300 MPa leads to a significant improvement of the FMLs' fatigue properties, increasing fatigue strength by at least 60 %, (test stopped at 160 MPa to not exceed the expected self-heating limit). In comparison to the non-post-stretched FML, the post-stretched shows a steady development of stiffness and strain up to 160 MPa without any signs of damage, which was confirmed by DIC deformation images. Applying fatigue stress on the FML, primarily in the tensile region of the aluminum sheet within plastic deformation, even though seeing no significant differences in stiffness as well as the relative changes in strain up to crack initiation, leads to accelerated crack initiation. This is delayed majorly by shifting the load on the aluminum sheet primarily to the elastic region between the compressive and tensile load capabilities using post-stretching.

The applied post-stretching determines the fatigue strength (Fig. 16), which is shown by the MAT results, indicated reliably by the change in testing frequency. Post-stretching up to 180 MPa is necessary, to increase the fatigue strength by 20 MPa, while 240 MPa post-stretching increases it by 50 MPa. Even though 300 MPa post-stretching increases it even further, there is a limit to post-stretching when the layer interface gets damaged, which hinders stress distribution between layers.

Since the MATs were conducted to gather knowledge about the effect of post-stretching in a short time and to estimate a fatigue strength

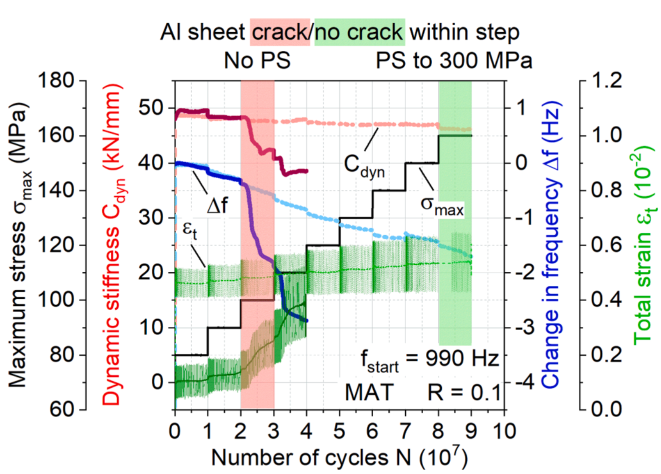

Fig. 15. Multiple amplitude test, starting at maximum stress of 80 MPa with a step width of 10^7 cycles, after which the maximum stress is increased by 10 MPa until 160 MPa. No post-stretching (PS) leads to early crack initiation, measurable at 100 MPa (highlighted in red), while the fiber metal laminate with 300 MPa post-stretching shows no signs of failure of the aluminum sheets for the whole test.

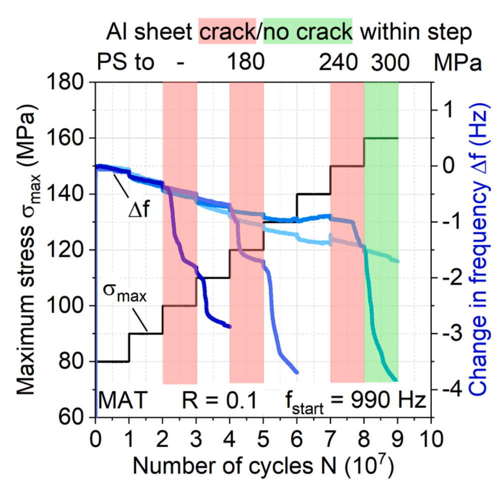

Fig. 16. Multiple amplitude test, starting at maximum stress of 80 MPa with a step width of 10^7 cycles, after which the maximum stress is increased by 10 MPa until 160 MPa. Post-stretching (PS), dependent on the height, can delay the time of crack initiation substantially.

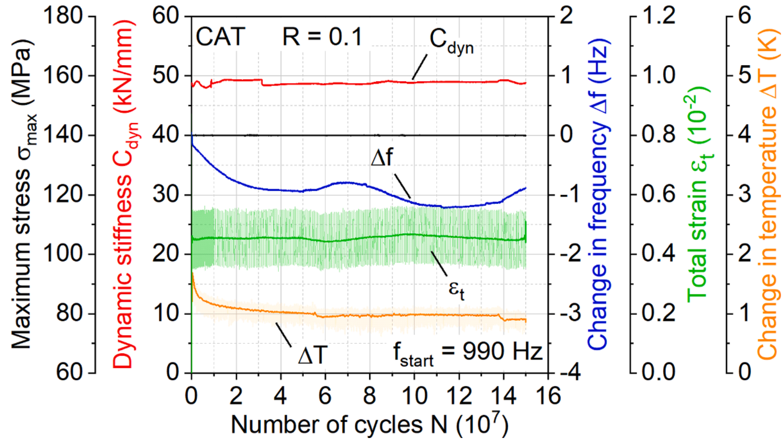

Fig. 17. Constant amplitude test at a maximum stress of 140 MPa on a 300 MPa post-stretched specimen. No aluminum sheet crack initiation was detected up to 1.5 × 10^8, where the test was stopped.

within the VHCF regime, CATs were conducted to validate the results. Fig. 17 shows an exemplary result for a CAT at a maximum stress of 140 MPa. The continuously constant progression of all the characteristic values shown (stiffness, frequency, strain, temperature) reflects the damage-free condition of the post-stretched specimen, until the stop of the test at 1.5 × 10^8 cycles. The periodical change in frequency can be attributed to the surrounding change in the temperature of testing machine parts, which is not visible in the measured temperature of the specimen due to temperature reference measurement compensation. Considering the low change in temperature compared to the relationship described in Section 3.3 (around 2 K expected at 140 MPa), the post-stretching induced change in strain behavior of the aluminum sheet reduces the amount of self-heating, enabling the FML to be tested with f ≈ 1,000 Hz up to aluminum cracking even at higher maximum stresses than investigated.

Fig. 18 essentially contains the data from Fig. 12, complemented with results on post-stretched FML to demonstrate the achieved increase in fatigue strength of the aluminum sheet component of the FML. Using post-stretching, at least 60 % increased fatigue strength of the aluminum sheets (green highlighted triangles), compared to non-post-stretched FML, is possible. There is a limit to such a lifetime extension, seeing that the course of the total FML failure (circles) inevitably crosses the course of the aluminum sheet cracking (triangles). Nevertheless, the FMLs' performance in a 300 MPa post-stretched state can rival established thermoset-based FMLs [4,7,60,63].

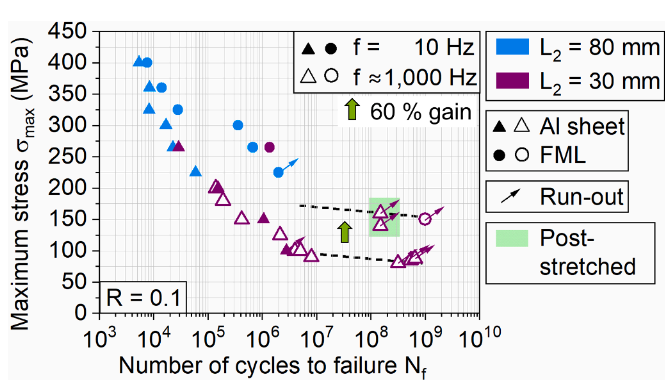

Fig. 18. S-N graph for thermoplastic-based fiber metal laminate (FML), complemented with results gathered from 300 MPa post-stretched FML. Data points contain experimental results gained from servo-hydraulic 10 Hz (filled data points) and high-frequency resonant ≈ 1,000 Hz (contour-bordered data points) testing. Triangles represent aluminum sheet cracking and circles total failure of the FML.

4. Conclusions and outlook

Using the testing methodology developed within this study, the characterization of the fatigue properties of thermoplastic-based hybrid fiber metal laminate up to the VHCF regime is possible within an efficient time frame. The combined utilization of high-speed digital image correlation with a 25 kHz frame rate for deformation measurements, enabling in-depth analysis of material-specific damage evolution, makes it attractive for general short-term material characterization for sustainable component design and dimensioning. Testing of the fiber metal laminate can be conducted using 1,000 Hz without significant changes in temperature. Within the gained results, no visible influence of strain rate was found. Multiple amplitude testing at 1,000 Hz enabled a fast and reliable estimation of the VHCF fatigue strength (around 90 MPa) while offering insight into the damage evolution. The damage mechanisms occurring within VHCF and HCF regimes are the same, but during VHCF load the number of initiating cracks as well as interlaminar delamination reduces. Using post-stretching, significant gains in fatigue strength of the fiber metal laminate are possible, increasing from 90 to at least 160 MPa, with regard to cracking of the aluminum sheet. Even if the aluminum sheets and the glass fiber-reinforced polyamide 6 layer fail within the VHCF regime, the carbon fiber-reinforced layer offers enough residual strength to secure the fiber metal laminate from total failure. These properties make it a creditable competitor in the area of fiber metal laminates with the advantages of formability, recyclability, and short consolidation cycle times for efficient mass production.

Nevertheless, important research topics are still open to being investigated. Even though post-stretching proved to be a valid method to improve the VHCF lifetime of the thermoplastic-based fiber metal laminate, the limits considering laminate integrity need to be quantified. In addition, the effect of post-stretching on the laminate's self-heating behavior at 1,000 Hz needs to be evaluated, since it may allow testing of the fiber metal laminate until aluminum sheet crack initiation at higher maximum stresses than initially expected. Further, the aluminum surface roughness influences the crack initiation, especially within the VHCF regime, and could be optimized for a prolonged lifetime. In this regard, fiber metal laminates with different aluminum surface treatments like anodizing or phosphating could be investigated concerning their VHCF performance. This should be complemented in total by the usage of application-oriented notch geometries to characterize the aluminum crack growth behavior. To expand the understanding of the thermoplastic-based fiber metal laminates' fatigue capabilities, more points need to be addressed. For example, the metal volume content, and layer stack-up of the laminate need to be considered for an in-depth investigation to determine their impact on fatigue life. Moreover, varying ambient temperatures (e.g., −35 and 80 °C) as well as ambient humidity, which affect the residual stress state of the FML as well as the polymer properties and therefore the damage evolution, are highly relevant. In this regard, enhancement of the surface-restricted measuring technologies (digital image correlation, thermography) through the usage of volume-based technology (e.g., computed tomography) will enable a quantifiable characterization of the volume-inner damage evolution, i.e., delamination growth.

CRediT authorship contribution statement

Selim Mrzljak: Writing – original draft, Visualization, Validation, Project administration, Methodology, Investigation, Data curation, Conceptualization. **Maik Trautmann:** Writing – original draft, Validation, Project administration, Methodology. **Guntram Wagner:** Writing – review & editing, Supervision, Resources, Funding acquisition. **Frank Walther:** Writing – review & editing, Supervision, Resources, Funding acquisition.

Declaration of competing interest

The authors declare that they have no known competing financial interests or personal relationships that could have appeared to influence the work reported in this paper.

Data availability

Data will be made available on request.

Acknowledgments

This work was funded by the German Research Foundation (Deutsche Forschungsgemeinschaft, DFG) within the research project "Mechanism-correlated characterization of the deformation and damage behavior of thermoplastic-based fiber metal laminates for property-oriented process development", project no. 414332488.

The authors thank the German Research Foundation and the Ministry of Culture and Science of North Rhine-Westphalia (Ministerium für Kultur und Wissenschaft des Landes Nordrhein-Westfalen, MKW NRW) for their financial support within the Major Research Instrumentation Program for the high-frequency resonant testing system Rumul Gigaforte 50, project no. 424760282, the high-speed camera system, project no. 424852613, the high-speed thermography system, project no. 444290516, and the in situ atomic force microscope, project no. 445052562.

We acknowledge financial support by the German Research Foundation and TU Dortmund University (Technische Universität Dortmund) within the funding program Open Access Costs.

References

[1] Kawai M, Hachinohe A. Two-stress level fatigue of unidirectional fiber-metal hybrid composite: GLARE 2. Int J Fatigue 2002;24:567–80. https://doi.org/10.1016/S0142-1123(01)00108-6.
[2] Kawai M, Kato K. Effects of R-ratio on the off-axis fatigue behavior of unidirectional hybrid GFRP/Al laminates at room temperature. Int J Fatigue 2006;28:1226–38. https://doi.org/10.1016/j.ijfatigue.2006.02.020.
[3] Alderliesten RC. Designing for damage tolerance in aerospace: a hybrid material technology. Mater Des 2015;66:421–8. https://doi.org/10.1016/j.matdes.2014.06.068.
[4] Asghar W, Nasir MA, Qayyum F, Shah M, Azeem M, Nauman S, et al. Investigation of fatigue crack growth rate in CARALL, ARALL and GLARE. Fatigue Fract Eng Mater Struct 2017;40:1086–100. https://doi.org/10.1111/ffe.12566.
[5] Deniz ME, Aydin F. Determination of fatigue life of the unidirectional GFRP/Al hybrid composite laminates. Compos B 2019;166:580–7. https://doi.org/10.1016/j.compositesb.2019.02.060.
[6] Dadej K, Bienas J, Surowska B. Residual fatigue life of carbon fibre aluminium laminates. Int J Fatigue 2017;100:94–104. https://doi.org/10.1016/j.ijfatigue.2017.03.026.
[7] Dadej K, Bienas J. On fatigue stress-cycle curves of carbon, glass and hybrid carbon/glass–reinforced fibre metal laminates. Int J Fatigue 2020;140:105843. https://doi.org/10.1016/j.ijfatigue.2020.105843.
[8] Vogelesang LB, Vlot A. Development of fibre metal laminates for advanced aerospace structures. J Mater Process Technol 2000;103:1–5. https://doi.org/10.1016/S0924-0136(00)00411-8.
[9] Kim CW, Oh DJ. Progressive delamination with and without crack propagation in aramid fiber reinforced metal laminates containing a circular notch. Mater Sci Eng A 2008;483–484:251–3. https://doi.org/10.1016/j.msea.2006.10.193.
[10] Alderliesten RC. Analytical prediction model for fatigue crack propagation and delamination growth in GLARE. Int J Fatigue 2007;29:628–46. https://doi.org/10.1016/j.ijfatigue.2006.07.006.
[11] Austin TSP, Singh MM, Gregson PJ, Powell PM. Characterisation of fatigue crack growth and related damage mechanisms in FRP-metal hybrid laminates. Compos Sci Technol 2008;68:1399–412. https://doi.org/10.1016/j.compscitech.2007.11.013.
[12] Nestler D, Trautmann M, Zopp C, Tröltzsch J, Osiecki T, Nendel S, et al. Continuous film stacking and thermoforming process for hybrid CFRP/aluminum laminates. Procedia CIRP 2017;66:107–12. https://doi.org/10.1016/j.procir.2017.03.221.
[13] Behrens B-A, Hübner S, Grbic N, Micke-Camuz M, Wehrhane T, Neumann A. Forming and joining of carbon-fiber-reinforced thermoplastics and sheet metal in one step. Procedia Eng 2017;183:227–32. https://doi.org/10.1016/j.proeng.2017.04.026.
[14] Harhash M, Fischer T, Grubenmann M, Hua W, Heingaertner J, Kuhtz M, et al. Top-hat crashboxes of thermoplastic fibre-metal-laminates processed in one-step thermoforming: Experimental and numerical study. Compos B 2021;226(109367):1–21. https://doi.org/10.1016/j.compositesb.2021.109367.
[15] Michel SA, Kieselbach R, Martens HJ. Fatigue strength of carbon fibre composites up to the gigacycle regime (gigacycle-composites). Int J Fatigue 2006;28(3):261–70. https://doi.org/10.1016/j.ijfatigue.2005.05.005.
[16] Wollmann T, Hahn M, Wiedemann S, Zeiser A, Jaschinski J, Modler N, et al. Thermoplastic fibre metal laminates: stiffness properties and forming behaviour by means of deep drawing. Arch Civ Mech Eng 2018;18:442–50. https://doi.org/10.1016/j.acme.2017.09.001.
[17] Mrzljak S, Trautmann M, Wagner G, Walther F. Influence of aluminum surface treatment on tensile and fatigue behavior of thermoplastic-based hybrid laminates. Materials 2020;13:2080. https://doi.org/10.3390/ma13143080.
[18] Cortes P, Cantwell WJ. The prediction of tensile failure in titanium-based thermoplastic fibre-metal laminates. Compos Sci Technol 2006;66:2306–16. https://doi.org/10.1016/j.compscitech.2005.11.031.
[19] Cortes P, Cantwell WJ. The fracture properties of a fibre-metal laminate based on magnesium alloy. Compos B 2006;37:163–70. https://doi.org/10.1016/j.compositesb.2005.06.002.
[20] Zopp C, Dittes A, Nestler D, Scharf I, Kroll L, Lampke T. Quasi-static and fatigue bending behavior of a continuous fiber-reinforced thermoplastic/metal laminate. Compos B 2019;174(107043):1–9. https://doi.org/10.1016/j.compositesb.2019.107043.
[21] Mrzljak S, Schmidt S, Kohl A, Hülsbusch D, Hausmann J, Walther F. Testing procedure for fatigue characterization of steel-CFRP hybrid laminate considering material dependent self-heating. Materials 2021;14:3394. https://doi.org/10.3390/ma14123394.
[22] Mrzljak S, Trautmann M, Blickling P, Wagner G, Walther F. Fatigue condition monitoring of notched thermoplastic-based hybrid fiber metal laminates using electrical resistance measurement and digital image correlation. J Compos Mater 2023;57(17):2669–87. https://doi.org/10.1177/00219983231176257.
[23] Hosoi A, Takamura K, Sato N, Kawada H. Quantitative evaluation of fatigue damage growth in CFRP laminates that changes due to applied stress level. Int J Fatigue 2011;33(6):781–7. https://doi.org/10.1016/j.ijfatigue.2010.12.017.
[24] Hülsbusch D, Helwing R, Mrzljak S, Walther F. Comparison of the damage evolution in glass fiber-reinforced polyurethane and epoxy in the HCF and VHCF regimes investigated by intermittent in situ x-ray computed tomography. In: IOP Conf Ser: Mater Sci Eng, 942; 2020, 012036. https://doi.org/10.1088/1757-899X/942/1/012036.
[25] Mayer H, Papakyriacou M, Pippan R, Stanzl-Tschegg SE. Influence of loading frequency on the high cycle fatigue properties of AlZnMgCu1.5 aluminium alloy. Mater Sci Eng A 2001;314:48–54. https://doi.org/10.1016/S0921-5093(00)01913-4.
[26] Zhu X, Jones J, Allison J. Effect of frequency, environment, and temperature on fatigue behavior of E319 cast aluminum alloy: stress-controlled fatigue life response. Metall Mater Trans A 2008;39:2681–8. https://doi.org/10.1007/s11661-008-9631-1.
[27] Mayer H, Schuller R, Fitzka M. Fatigue of 2024–T351 aluminum alloy at different load ratios up to 1010 cycles. Int J Fatigue 2013;57:113–9. https://doi.org/10.1016/j.ijfatigue.2012.07.013.
[28] Flore D, Wegener K, Mayer H, Karr U, Oetting CC. Investigation of the high and very high cycle fatigue behaviour of continuous fibre reinforced plastics by conventional and ultrasonic fatigue testing. Compos Sci Technol 2017;141:130–6. https://doi.org/10.1016/j.compscitech.2017.01.018.
[29] Stanzl-Tschegg SE, Papakyriacou M, Mayer HR, Schijve J, Tschegg EK. High-cycle fatigue crack growth properties of aramid-reinforced aluminum laminates. Compos Mater Fatigue Fract, ASTM STP 1993;1156(4):637–52. https://doi.org/10.1520/STP24755S.
[30] Papakyriacou M, Schijve J, Stanzl-Tschegg SE. Fatigue crack growth behaviour of fibre-metal laminate GLARE-1 and metal laminate 7475 with different blunt notches. Fatigue Fract Engng Mater Struct 1997;29(11):1573–84. https://doi.org/10.1111/j.1460-2695.1997.tb01512.x.
[31] Stanzl-Tschegg SE. Fracture mechanisms and fracture mechanics at ultrasonic frequencies. Fatigue Fract Engng Mater Struct 2001;22:567–79. https://doi.org/10.1046/j.1460-2695.1999.00180.x.

[32] Ilie P, Lesperance X, Ince A. Development of an ultrasonic fatigue testing system for gigacycle fatigue. Mater Des Process Commun 2019;2(6):1–9. https://doi.org/10.1002/mdp2.120.

[33] Weibel D, Beck T, Balle F. Fatigue properties and damage of CF-PPS from high to very high cycles. In: Proceedings of the 22nd International Conference on Composite Materials. (2019) 1-7.

[34] Ritchie RO, Davidson DL, Boyce BL, Campbell JP, Roder O. High-cycle fatigue of Ti-6Al-4V. Fatigue Fract Engng Mater Struct 1991;22:621–31.

[35] Liaw PK, Wang H, Jiang L, Yang B, Huang JY, Kuo RC, et al. Thermographic detection of fatigue damage of pressure vessel steels at 1,000 Hz and 20 Hz. Scr Mater 2000;42(4):389–95. https://doi.org/10.1016/S1359-6462(99)00358-9.

[36] Krupp U, Giertler A, Marinelli MC, Dönges B, Knobbe H, Christ H-J. Evaluation of microstructural barriers during fatigue damage of duplex stainless steels at very high cycles. Materials Testing 2012;54:564–8. https://doi.org/10.3139/120.110366.

[37] Smaga M, Boemke A, Daniel T, Skorupski R, Sorich A, Beck T. Fatigue behavior of metastable austenitic stainless steels in LCF, HCF and VHCF regimes at ambient and elevated temperatures. Metals 2019;9(6):704. https://doi.org/10.3390/met9060704.

[38] Schopf T, Weihe S, Daniel T, Smaga M, Beck T. Fatigue behavior and lifetime assessment of an austenitic stainless steel in the VHCF regime at ambient and elevated temperatures. Fatigue Fract Eng Mater Struct 2023;46:1763–74. https://doi.org/10.1111/ffe.13958.

[39] Zeuner AT, Kühne R, Standke C, Köberlin D, Wanski T, Schettler S, et al. Fatigue behavior of laser-cut sheet metal parts with brazed-on elements. Metals 2021;11(12):2063. https://doi.org/10.3390/met11122063.

[40] Kuliiev R, Riekehr S, Ventzke V, Keller S, Kashaev N. On the effect of testing frequency on high and very high cycle fatigue behavior of AA2024-T3, Ti-6Al-4V, and Inconel 718. J Mater Eng Perform 2023;32:10843–56. https://doi.org/10.1007/s11665-023-08385-4.

[41] Fitzka M, Mayer H. Constant and variable amplitude fatigue testing of aluminum alloy 2024–T351 with ultrasonic and servo-hydraulic equipment. Int J Fatigue 2016;91:363–72. https://doi.org/10.1016/j.ijfatigue.2015.08.017.

[42] Schneider J, Bödecker J, Berger C, Oechsner M. Frequency effect and influence of testing technique on the fatigue behaviour of quenched and tempered steel and aluminium alloy. Int J Fatigue 2016;93:224–31. https://doi.org/10.1016/j.ijfatigue.2016.05.013.

[43] Tenkamp J, Awd M, Siddique S, Starke P, Walther F. Fracture-mechanical assessment of the effect of defects on the fatigue lifetime and limit in cast and additively manufactured aluminum-silicon alloys from HCF to VHCF regime. Metals 2020;10(7):943. https://doi.org/10.3390/met10070943.

[44] Hertzberg RW, Manson JA, Skibo M. Frequency sensitivity of fatigue processes in polymeric solids. Polym Eng Sci 1975;15(4):252–60. https://doi.org/10.1002/pen.760150404.

[45] Mandell J, Meier U. Effects of stress ratio, frequency, and loading time on the tensile fatigue of glass-reinforced epoxy. In: Long-Term Behavior of Composites. West Conshohocken, USA: ASTM International; 1983. p. 55–77. https://doi.org/10.1520/STP31816S.

[46] Perreux D, Joseph E. The effect of frequency on the fatigue performance of filamentwound pipes under biaxial loading: Experimental results and damage model. Compos Sci Technol 1997;57(3):353–64. https://doi.org/10.1016/S0266-3538(96)00155-8.

[47] Parsons M, Stepanov EV, Hiltner A, Baer E. Effect of strain rate on stepwise fatigue and creep slow crack growth in high density polyethylene. J Mater Sci 2000;35(8):1857–66. https://doi.org/10.1023/A:1004741713514.

[48] Alpinis R. Acceleration of fatigue tests of polymer composite materials by using high frequency loadings. Mech Compos Mater 2004;40:107–18. https://doi.org/10.1023/B:MOCM.0000025485.93979.dd.

[49] Hahn TH, Turkgenc O. The effect of loading parameters on fatigue of composites laminates: Part IV information systems. U.S. Department of Transportation. Washington D.C., USA, DOT/FAA/AR-00/48; 2000.

[50] Barron V, Buggy M, McKenna NH. Frequency effects on the fatigue behaviour on carbon fibre reinforced polymer laminates. J Mater Sci 2001;36(7):1755–61. https://doi.org/10.1023/A:1017576725885.

[51] Ružek R, Kadlec M, Petrusová L. Effect of fatigue loading rate on lifespan and temperature of tailored blank C/PPS thermoplastic composite. Int J Fatigue 2018;113:253–63. https://doi.org/10.1016/j.ijfatigue.2018.04.023.

[52] Adam TJ, Horst P. Very high cycle fatigue testing and behavior of GFRP cross- and angle-ply laminates. Fatigue of Materials at Very High Numbers of Loading Cycles. Springer Spektrum. Wiesbaden, (2018) 511-532. https://doi.org/10.1007/978-3-658-24531-3_23.

[53] Vieille B, Taleb L. High-temperature fatigue behavior of woven-ply thermoplastic composites. In: Fatigue Life Prediction of Composites and Composite Structures. Duxford, UK: Woodhead Publishing; 2019. p. 195–238. https://doi.org/10.1016/B978-0-08-102575-8.00006-1.

[54] Jeannin T, Gabrion X, Ramasso E, Placet V. About the fatigue endurance of unidirectional flax-epoxy composite laminates. Compos B Eng 2019;165:690–710. https://doi.org/10.1016/j.compositesb.2019.02.009.

[55] Kappel E, Prussak R, Wiedemann J. On a simultaneous use of fiber-Bragg-gratings and strain-gages to determine the stress-free temperature Tsf during GLARE manufacturing. Compos Struct 2019;227(111279):1–10. https://doi.org/10.1016/j.compstruct.2019.111279.

[56] Vogelesang LB, Gunnink JW. ARALL, a material for the next generation of aircraft. A state of the art. Delft University of Technology. Report LR-400; 1983. http://resolver.tudelft.nl/uuid:3334f1f9-aa5c-4a1f-a8c8-c58b4c3f821e.

[57] R.C. Alderliesten. Fatigue crack propagation and delamination growth in GLARE. Dissertation. (2005). Delft University Press. ISBN 90-407-2588-8. http://resolver.tudelft.nl/uuid:15006e44-1232-4ef2-87bd-776b249d61f5.

[58] Lee B-E, Park E-T, Kim J, Kang B-S, Song W-J. Analytical evaluation on uniaxial tensile deformation behavior of fiber metal laminate based on SRPP and its experimental confirmation. Compos B 2014;67:154–9. https://doi.org/10.1016/j.compositesb.2014.06.031.

[59] Zhang X, Meng W, Guo J, Zhang Y. Available relevant study on stress analysis and static strength prediction of fiber metal laminates. Scanning 2020. https://doi.org/10.1155/2020/8874830.

[60] Khan SU, Alderliesten RC, Benedictus R. Post-stretching induced stress redistribution in fibre metal laminates for increased fatigue crack growth resistance. Compos Sci Technol 2009;69:396–405. https://doi.org/10.1016/j.compscitech.2008.11.006.

[61] Trautmann M, Mrzljak S, Walther F, Wagner G. Mechanical properties of thermoplastic-based hybrid laminates with regard to layer structure and metal volume content. Metals 2020;10:1430. https://doi.org/10.3390/met10111430.

[62] Hausmann J, Naghipour P, Schulze K. Analytical and numerical residual stress models for fiber metal laminates - comparison and application. Procedia Mater Sci 2013;2:68–73. https://doi.org/10.1016/j.mspro.2013.02.009.

[63] Plokker HM, Alderliesten RC, Benedictus R. Crack closure in fibre metal laminates. Fatigue Fract Eng Mater Struct 2007;30(7):608–20. https://doi.org/10.1111/j.1460-2695.2007.01140.